Nano Research

Open Access

Research Article

A universal approach for extraction of single-walled carbon nanotubes of specific chirality using aqueous two-phase extraction

Błażej Podleśny[1] ✉, Łukasz Czapura[1], Patrycja Taborowska[1], Luyao Zhang[2], Feng Yang[2], and Dawid Janas[1] ✉

[1] *Department of Organic Chemistry, Bioorganic Chemistry and Biotechnology, Silesian University of Technology, 44–100 Gliwice, Poland*
[2] *Department of Chemistry, Southern University of Science and Technology, Shenzhen 518055, China*

Cite this article: *Nano Research*, **2025**, *18*, 94907112. https://doi.org/10.26599/NR.2025.94907112

ABSTRACT: The development of effective methods for obtaining monochiral single-walled carbon nanotubes (SWCNTs) is necessary to make many applications based on them viable for everyday use. Large-diameter semiconducting SWCNTs are particularly valuable due to their low band gap, but the isolation of such SWCNTs remains difficult to achieve as the number of possible chiralities scales strongly with diameter, and there are an overwhelming number of large-diameter SWCNT types. In this study, we demonstrate how monochiral (8,6) SWCNTs, which are 0.966 nm in diameter, can be straightforwardly harvested using the aqueous two-phase extraction (ATPE) method by employing a combination of ionic and non-ionic surfactants. The universal nature of the devised technique was demonstrated by generating fractions enriched with (8,6) SWCNTs starting from various commercially available mixtures of SWCNTs with drastically different compositions. To demonstrate the practical utility of the generated material, we studied how the obtained pure SWCNTs may be chemically modified to improve their optical characteristics. Interestingly, the course of the functionalization was highly dependent on the type of dispersant used to suspend the purified SWCNTs in the aqueous medium.

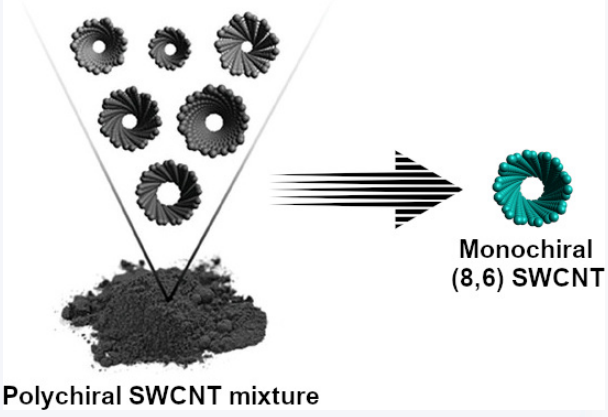

KEYWORDS: single-walled carbon nanotubes, purification, functionalization, sensing

1 Introduction

Single-walled carbon nanotubes (SWCNTs) have been an attractive research object for over thirty years [1]. However, despite this popularity, sufficiently selective, scalable, and inexpensive methods for the synthesis of SWCNTs of particular chiralities have not yet been developed. Therefore, unless the produced polychiral SWCNTs are sorted, they comprise multiple different species, each of which exhibits different characteristics, dramatically decreasing the application potential of the blended material [2]. However, given the very small size of SWCNTs, differentiation of the material is non-trivial. As the number of possible SWCNT configurations scales with their diameter [3], typically employed raw materials, such as HiPco SWCNTs and Tuball SWCNTs, are extremely heterogeneous. Considering their diameter distribution, these unprocessed SWCNT sources may, in theory, contain up to 43 and 130 chiralities, making their purification very challenging (cf. Electronic Supplementary Material (ESM) file to learn more about this estimation). Nonetheless, because these polychiral SWCNT sources are available in large quantities at a reasonable cost, the development of techniques for the isolation of desired species from such parent materials is essential.

Currently, differentiation of SWCNTs can be achieved using a spectrum of methods, such as electrophoresis [4], density gradient ultracentrifugation (DGU) [5], conjugated polymer extraction (CPE) [6], chromatography [7], and aqueous two-phase extraction (ATPE) [8]. The latter one has recently received considerable interest from the scientific community [2, 8] due to its simple protocol and low entry barrier, as it does not necessitate the use of any non-standard laboratory equipment [9, 10]. In brief, this technique hinges upon the creation of two immiscible aqueous phases between which SWCNTs can be partitioned [9, 10]. The introduction of specific compounds, such as surfactants [11–14], inorganic salts [15, 16], acids/bases [17, 18], etc., promotes the migration of SWCNTs between the phases, thereby enabling their

Received: September 20, 2024; **Revised:** October 24, 2024
Accepted: November 4, 2024

✉Address correspondence to Błażej Podleśny, Blazej.Podlesny@polsl.pl; Dawid Janas, Dawid.Janas@polsl.pl

stepwise purification. The almost unlimited possibility of tuning the extraction systems has made it possible to extract SWCNTs using the ATPE method due to their electrical nature [19, 20], diameter [21], chirality [22, 23], or handedness [24].

Nevertheless, most of the published studies on the separation of SWCNTs are related to processing materials containing predominantly small-diameter SWCNTs, commonly those already enriched with certain SWCNT types at the synthesis stage, such as (6,5) or (7,6), which simplifies the purification [23, 25]. While initially, most of the publications reported metallic/semiconducting SWCNT separation [19, 20, 26, 27], ultimately, the isolation of monochiral SWCNTs was also achieved [18, 22, 24, 28, 29]. However, to isolate monochiral SWCNTs with diameters larger than 1 nm, one typically needs to exploit specific interactions of deoxyribonucleic acids with SWCNTs. This approach, however, suffers from relatively large costs and the inferior stability of DNA in the ambient systems [22]. Concomitantly, the combined application of less sophisticated compounds, such as surfactants and partitioning modulators (e.g., KSCN), in the biphasic purification can also produce SWCNT suspensions in which certain large-diameter SWCNT types are abundant [14, 16]. Recently, high-resolution extraction of large-diameter SWCNTs was achieved when they were subjected to endohedral filling with hexadecane [18]. Unfortunately, filled SWCNTs are not always desirable for specific applications. In light of the preceding considerations, there is a scarcity of protocols with few steps for the separation of unmodified near-monochiral large-diameter SWCNTs using the classical ATPE, which would be free of the limitations imposed by employing DNA.

Other SWCNT differentiation methods are also not sufficiently helpful in this context. For instance, CPE, despite its capacity to provide small monochiral (6,5) [30], (7,3) [6], and (7,5) [31] SWCNTs, is not analogously valuable in the large-diameter regime. Typically, for large-diameter SWCNTs, it is only capable of discriminating between semiconducting and metallic SWCNTs, while the generated fractions have a polychiral nature. For instance, the polymers based on a carbazole or fluorene unit enabled the metallic/semiconducting separation of a mixture of SWCNTs with diameters exceeding 1.2 nm [32, 33]. Similarly, the application of a polymer based on the diketopyrrolopyrrole motif resulted in the extraction of SWCNTs with diameters higher than 1.5 nm [34]. Further advances in this area resulted in the enrichment of the generated fractions with SWCNTs of large diameters, such as (10,8) SWCNTs/(12,5) SWCNTs [32] and (15,4) SWCNTs [35, 36] (1.24, 1.20, and 1.38 nm, respectively). Nonetheless, the provided optical absorption spectra revealed the presence of various species in the obtained SWCNT suspensions. Despite the benefits of using CPE, one issue remains unresolved, which is the difficulty in removing the polymer molecules from the SWCNT surface [37]. Complete purification of chirality-enriched SWCNTs from this contamination is challenging and negatively affects the total yield of the purification process. This, in turn, very much reduces the application potential of such SWCNTs in many important fields of exploitation, e.g., nanomedicine [38, 39]. Therefore, until effective techniques for the liberation of sorted SWCNTs from the polymer molecules are developed, it is essential to increase the resolution of the ATPE method, which provides materials that can be straightforwardly isolated from the compounds in the process mixture used for the partitioning.

In this study, we present how the separation of large-diameter SWCNTs with the ATPE method can be accomplished. The methodology devised herein enabled the extraction of near-monochiral (8,6) SWCNTs in only three steps using a dextran-poly(ethylene glycol) biphasic system, in which the movement of SWCNTs between the phases was directed by sodium deoxycholate and Brij35. The versatility of the developed method was confirmed by processing four commercially available SWCNT mixtures. Interestingly, the abovementioned SWCNT type was harvested even from a particular raw material that should not contain this SWCNT type according to its reported diameter distribution. Besides that, we devised a tactic enabling convenient purification of the chirality-enriched materials from the post-separation solutions using simple laboratory techniques. To demonstrate the utility of the extracted material, the obtained chirality-enriched SWCNTs were functionalized using diazonium chemistry with the aim of enriching their optical characteristics. Notably, the presence of particular surfactant combinations strongly affected the outcome of the chemical modification. Finally, we displayed the possibility of using functionalized (8,6) SWCNTs in ratiometric sensing of Vitamin C (VC).

2 Results and discussion

2.1 Partitioning of large-diameter SWCNT mixture

For the separation, we used a well-known system consisting of dextran (DEX) and polyethylene glycol (PEG) (Table S3 in the ESM), readily capable of differentiating SWCNTs [12]. A non-ionic surfactant (Brij35) was used to promote the SWCNT separation following our recent findings that non-ionic surfactants are very successful in discriminating between SWCNTs by diameter [12, 13]. SWCNT suspensions were prepared using sodium cholate (SC) or sodium deoxycholate (DOC), while SC/DOC, in conjunction with Brij35 were used to sort the SWCNTs. Both bile salt surfactants provided a satisfactory degree of SWCNT solubilization (Fig. S1(a) in the ESM). Based on the obtained spectra, it was evident that the raw material contained a multitude of different SWCNT species that could not be assigned specific SWCNT chiralities with certainty. The evaluation of SC@SWCNT and DOC@SWCNT suspensions indicated that the former one was unsuitable for further experiments under the selected conditions as the SWCNTs did not occupy the bottom phase, so they could not be shifted upward by the non-ionic Brij35 (Fig. S1(b) in the ESM). Therefore, we used SWCNT suspensions prepared in DOC for further experiments. To shed more light on the composition of the DOC@SWCNTs, we subjected them to photoluminescence (PL) excitation–emission mapping (Fig. S2 in the ESM). To our surprise, we noted the presence of many small SWCNT species that were outside of the SWCNT diameter distribution (1.6 ± 0.4 nm) disclosed by the manufacturer [40]. This result encouraged us to probe the possibility of partitioning this SWCNT population.

After the first extraction step, we obtained two highly colored phases (a brownish upper and a bluish lower phase); both of these had high SWCNT concentrations, as the colors were visible only after dilution (Fig. S3 in the ESM). Suspecting that the DOC/Brij35 system should offer diameter-based separation, with larger SWCNTs occupying the top phase [12], we characterized the obtained material by PL mapping (Figs. 1(a)–1(c)).

The lack of PL signals in the first top phase fraction (T1), with the concurrent abundance of peaks from smaller-diameter SWCNT species in the bottom-phase fraction (B1), indicated that the upper fraction was predominantly composed of large-diameter metallic

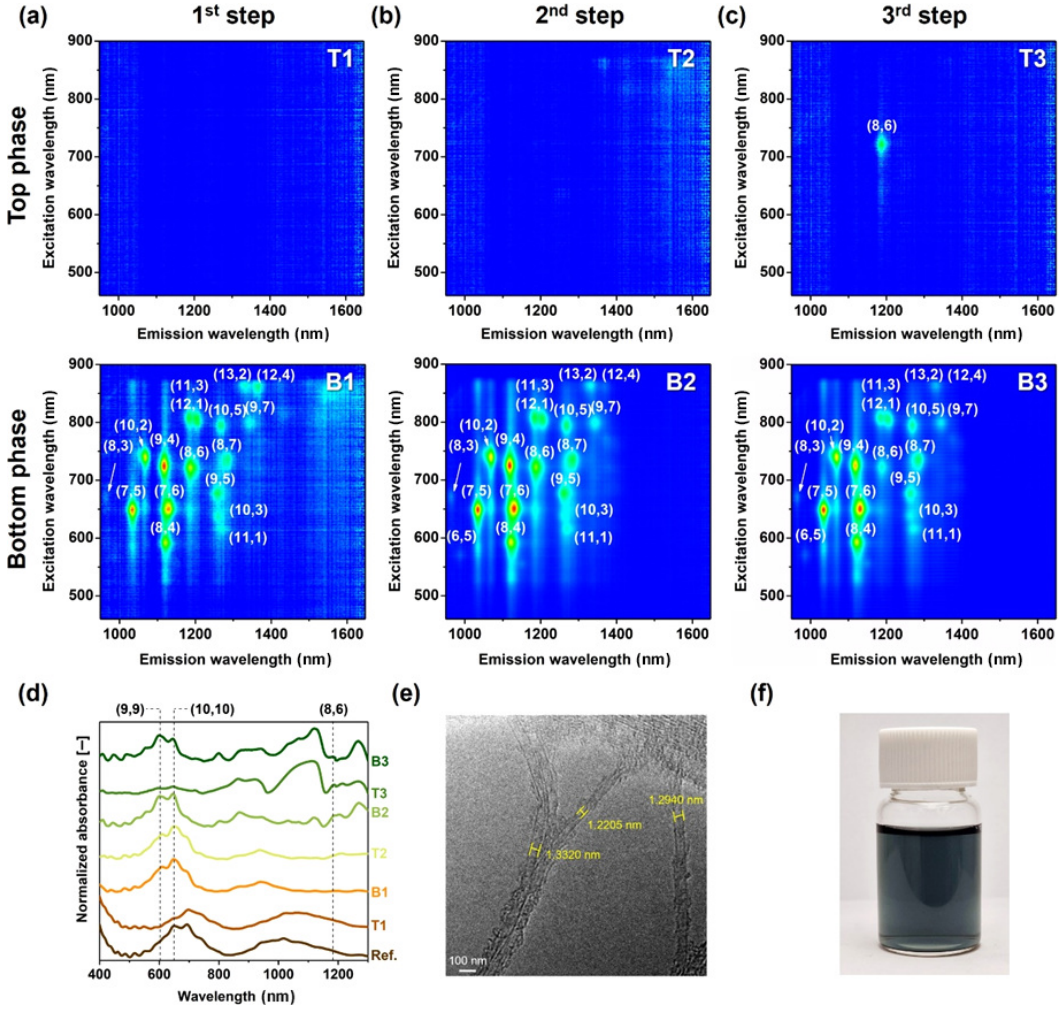

Figure 1 Characterization of the samples obtained from processing of large-diameter SWCNT raw material (Tuball). (a)–(c) PL excitation–emission maps of top and bottom phases after each separation step. (d) Corresponding optical absorption spectra, (e) TEM images, and (f) photograph of purified B1 sample.

and semiconducting SWCNTs. The PL emission from the latter either extended beyond the measurement window of the available apparatus, or they were not evident due to the much lower PL quantum yield (PLQY) of such large-diameter species [41].

Additional characterization by optical absorbance spectroscopy validated these conclusions (Fig. 1(d)). The spectrum of the top phase from the first separation step resembled the spectrum of the raw material, which was redshifted, indicating extraction of the population of the largest SWCNTs. Concomitantly, the bottom phase spectrum displayed a blueshift, corroborating the enrichment of the generated suspension with smaller semiconducting SWCNTs than the ones typically present in the raw material, along with the presence of some metallic SWCNTs. Regarding this fraction, two distinct peaks centered at 611 and 649 nm were noted, which likely corresponded to (9,9) and (10,10) SWCNTs (1.238 and 1.375 nm diameters, respectively), in addition to the smaller diameter semiconducting SWCNTs [14]. This assignment was also indirectly supported by the color of the sample (Fig. S3(c) in the ESM), which matched previous reports documenting the visual appearance of suspensions of such SWCNT types [24].

Using the bottom phase from the first step (B1), containing these two SWCNT types and a wide spectrum of semiconducting SWCNT species, we carried out subsequent separation to improve the partitioning of the semiconducting SWCNTs and reduce the content of metallic ones (Fig. 1(b)). The procedure (Table S4 in the ESM) involved combining the non-diluted bottom phase (B1) with a PEG solution to create a biphasic system, along with water and the DOC/Brij35 solutions, to reach a satisfactory degree of partitioning. After homogenization and centrifugation, the sample split into a light bluish upper phase (T2) and a greyish blue bottom phase (B2). We characterized the obtained phases, and, to our satisfaction, the T2 fraction was enriched in metallic SWCNTs as the recorded PL map again did not contain any peaks, while the optical absorption spectrum mainly contained peaks coming from (9,9) SWCNTs and (10,10) SWCNTs. Conversely, for the B2 phase, both the PL map and the optical absorption spectrum revealed the highly polychiral nature of the material, which contained a plethora of semiconducting SWCNTs.

Finally, we proceeded to the ultimate separation of the B2 phase. The results of PL excitation–emission mapping (Fig. 1(c)) indicated the emergence of (8,6) SWCNTs in the T3 phase. Since, as previously discussed, the DOC/Brij35 system should discriminate between SWCNTs by diameter, it was an unexpected outcome because this was not the largest semiconducting SWCNT type present in B2, yet it was preferentially shifted to the top phase. Nonetheless, even though the characterization of the material by PL suggested a monochiral character of the sample (Figs. 1(a)–1(c)), the corresponding optical absorption spectrum (Fig. 1(d))

uncovered that, in reality, the sample was much more heterogeneous. Unfortunately, due to the relatively low concentration of SWCNTs in this fraction, the spectrum was unclear, and accurate determination of the composition of the material was impossible. These results strongly suggested that using another SWCNT material of different composition, richer in (8,6) SWCNTs, was justified, and the results of such experiments are presented later in the text.

To elucidate the trend of SWCNT migration in the biphasic system, we employed Raman spectroscopy. We focused on the analysis of the radial breathing mode (RBM) area, which enables the estimation of the diameter distribution of the SWCNTs excited with light of a particular wavelength [42, 43]. We interpreted the Raman spectra of the raw material as well as that of the SWCNTs obtained after the first separation step. We only examined samples after the first step because they were sufficiently concentrated and, besides, the shapes of their absorption spectra were significantly different from each other, which should enable convenient interpretation of Raman spectra. Firstly, the recorded data (Fig. S4 and Table S5 in the ESM) confirmed that, in general, the SWCNTs were distributed between the phases according to diameter. Clearly, the largest SWCNTs occupied the top phase after the first partitioning step, validating our hypothesis about the diameter-dependent shift of SWCNTs from the bottom to the top, starting with the largest species. Secondly, Raman analysis corroborated our previous reasoning about the composition of the B1 phase, confirming the presence of the suspected metallic SWCNT types, i.e., (9,9) and (10,10) species. To verify the enrichment of the B1 fraction (and samples derived from it) in metallic (9,9) and (10,10) SWCNT, we analyzed the SWCNT diameter using transmission electron microscopy (TEM). Satisfactorily, the diameters of the examined SWCNTs stayed in accordance with the diameters (1.2–1.3 nm) of the suspected (9,9) and (10,10) SWCNTs (Fig. 1(e)). Additionally, the fraction containing these SWCNT species had a dark blue color, as expected (Fig. 1(f)).

2.2 Enhancement of the yield of extraction of (8,6) SWCNTs

In the previous part of the manuscript, we showed the possibility of a three-step extraction leading to an increased concentration of (8,6) SWCNTs in the top phase. However, even though the PL map detected only this chirality, the optical absorbance spectrum revealed that the collected fraction was of low concentration and also contained other SWCNT types. Undeniably, monochiral (8,6) species is a valuable SWCNT type because of its desirable spectroscopic properties. The wavelengths of maximum optical absorbance for both the S_{11} and S_{22} transitions are situated in the *in vivo* imaging window (second and first, respectively) [44]. Hence, to achieve a higher extraction yield of this valuable SWCNT type, we decided to sort raw SWCNTs containing a higher content of such SWCNTs. The widely studied (6,5)-enriched CoMoCAT SWCNT, (7,6)-enriched CoMoCAT SWCNT, and HiPco SWCNT materials were selected for this purpose. The mean diameter values of the first two were 0.76 and 0.9 nm [45], respectively, whereas the latter had a diameter distribution of 0.8–1.2 nm [46] (Fig. 2).

The experiments were first conducted on the (6,5)-enriched CoMoCAT SWCNTs (CoMoCAT65), containing perhaps the smallest number of SWCNT species among all the commercially available raw SWCNTs. Although (8,6) SWCNTs were not pronounced in the optical absorbance spectrum (Fig. S8 in the ESM) and the PL excitation–emission map (Fig. 2), we nonetheless carried out a three-step extraction analogously to that performed previously for large-diameter SWCNTs (Tuball), which comprised a greater number of larger SWCNT species. The PL excitation–emission maps of the resulting bottom phases did not differ significantly from each other and from the starting material (Fig. S9 in the ESM), whereas the data for the top phases indicated a gradual change in composition with each partitioning step. Interestingly, (8,6) SWCNTs were already detected in the T2 phase. Unfortunately, all the top phases (T1–T3) contained mostly (6,5) SWCNTs, which, as the tradename suggests, are abundant in this type of material. The collected fractions also displayed a relatively

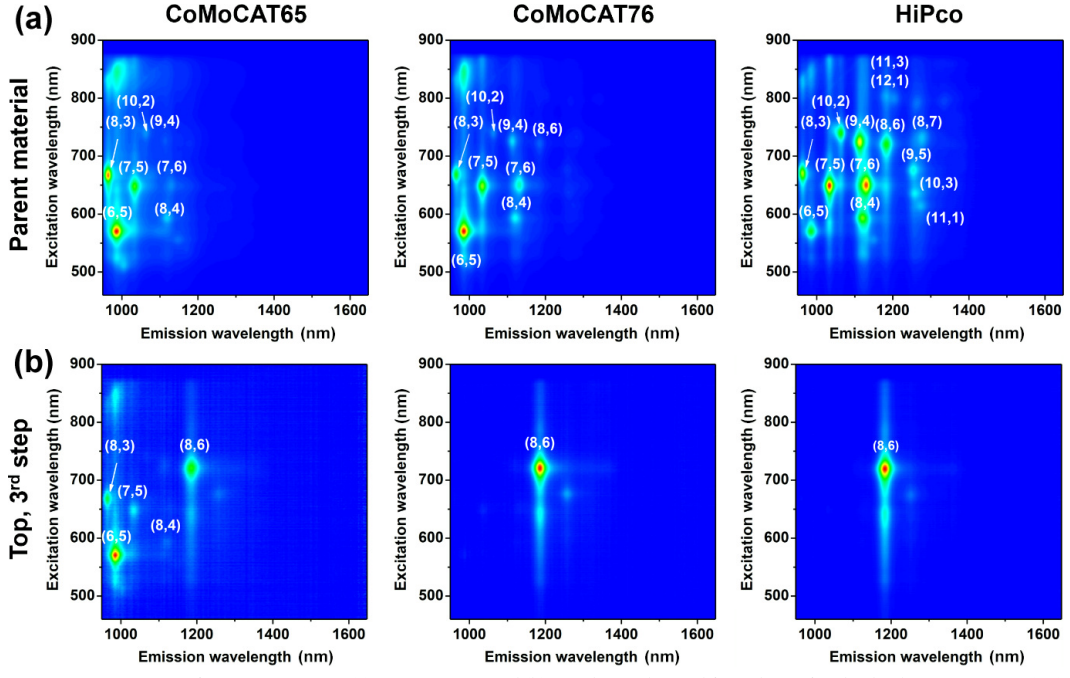

Figure 2 PL excitation–emission maps of various SWCNTs. (a) raw SWCNTs and (b) top phases obtained from them after the third separation step (T3).

low concentration of SWCNTs, which was reflected in poorly resolved optical absorbance spectra (Fig. S10 in the ESM).

These unsatisfactory results prompted us to examine another starting material, also produced by the CoMoCAT method, comprising slightly larger SWCNTs. The (7,6)-enriched raw SWCNT soot (CoMoCAT76) contained a wider spectrum of chiralities, including the desired (8,6) species (Fig. 2 and Fig. S11 in the ESM), which should facilitate a more effective extraction of this chirality. Hence, similarly to before, we carried out a three-step extraction using the same conditions. Again, the PL excitation–emission maps of the bottom phases did not differ much from each other, while the dissimilarities were more noticeable between the created top phase fractions (Fig. S11 in the ESM). In the upper phase after the first stage, T1, only weak, residual signals of SWCNTs were detected. Subsequently, in T2, (8,6) SWCNTs and (10,3) SWCNTs were the dominant SWCNT types registered. Finally, after the third extraction step, an almost monochiral fraction of (8,6) SWCNTs was collected in T3. The optical absorbance spectra were in line with these results (Fig. S12 in the ESM).

Encouraged by these outcomes, we employed raw SWCNTs of even larger mean diameter, i.e., HiPco SWCNTs, and sorted them accordingly, assuming that such material should provide the greatest number of the desired SWCNT type. Compared with the previously studied CoMoCAT SWCNTs, this material had a notably large share of species with large diameters, such as (7,5), (7,6), and (9,4) SWCNTs (Fig. 2). To our delight, enrichment of (8,6) SWCNTs using the developed routine was most successful for this type of raw material, even in the more evident presence of species with diameters similar to (8,6) SWCNTs, such as (10,3), (9,5), or (12,1) in the parent material. After the second extraction step, the top phase fraction T2 contained (8,6) and (10,3) SWCNTs (Figs. S13 and S14 in the ESM), but the following separation round made the T3 sample much more enriched with (8,6) SWCNTs. According to the PL excitation–emission map shown above, it could be customarily classified as monochiral.

To validate the possibility of upscaling the newly developed method of (8,6) SWCNT harvesting, we first tuned the separation conditions using the much more inexpensive Tuball SWCNTs. To reach this objective, we increased the initial overall concentration of SWCNTs in the dispersion (0.25 mg/mL) used for sorting by two and four times and carried out three-step extractions using raw SWCNT dispersions with concentrations of 0.25, 0.50, and 1.0 mg/mL. The desired SWCNT type was enriched in T3 (Fig. S15 in the ESM), and the concentration increase proportionally improved the capacity of the system to generate purified (8,6) SWCNTs. Based on this success, we returned to the processing of more suitable HiPco SWCNTs containing a larger share of the targeted chirality. Processing of the concentrated SWCNT suspension (1.0 mg/mL) led to a satisfactory level of purity being reached, according to the acquired PL excitation–emission maps (Fig. S16 in the ESM) and optical absorbance spectra (Fig. S17 in the ESM). Having established an optimized technique to obtain sufficiently pure SWCNT fractions of a relatively uncommon SWCNT type, we subsequently evaluated its application potential.

2.3 Chemical modification of isolated (8,6) SWCNTs

It is commonly known that implantation of sp^3 defects improves the optical characteristics of SWCNTs, producing a new defect-induced emission feature E_{11}^* [47], red-shifted with respect to the inherent E_{11} optical transition, which, under specific conditions, increases the PLQY of the material [48]. The optical emission of (8,6) SWCNTs is positioned relatively far into the near-infrared range (ca. 1182 nm), so having the ability to produce an even more redshifted peak by exercising chemical modification may make the material more applicable in telecommunications because the emission band of functionalized (8,6) SWCNTs is coherent with the O-band (referred to as the original band) [49]. To achieve this, we used 4-bromobenzendiazonium tetrafluoroborate (PhBr-Dz), which is a popular reagent employed to introduce sp^3 luminescent defects into the hexagonal lattices of SWCNTs [47]. During the research, we studied not only the simple influence of regent concentration and reaction time, but also the role of the surfactants present in the sample.

Our first attempt involved combining the SWCNT post-extraction suspension comprising phase-forming compounds (PEG, DEX) and surfactants (DOC, Brij35), to which neat PhBr-Dz solution was added. The reaction mixture was then kept in the dark, according to the established procedure for the functionalization of SWCNTs with small diameters [47, 50] (Fig. 3). Surprisingly, (8,6) SWCNTs, despite their large diameter, showed signs of functionalization immediately after the introduction of the functionalizing agent, giving a small rise in intensity of the E_{11}^* peak compared with the reference, which did not exhibit any development of the E_{11}^* feature in the absence of the diazonium salt (Fig. 3(a)). With time, the E_{11}^* intensity gradually increased, eventually reaching an E_{11}/E_{11}^* ratio of 0.79 after 2.5 h since the PhBr-Dz was added.

Larger diameter SWCNTs are less reactive compared to the smaller ones, because of their smaller curvature. Hence, a form of stimulation such as irradiation is sometimes employed to tackle this problem [51]. However, we still observed a successful grafting of

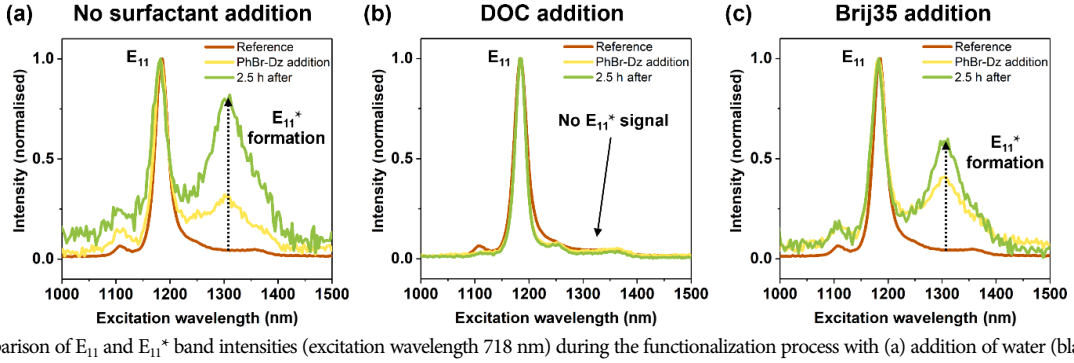

Figure 3 Comparison of E_{11} and E_{11}^* band intensities (excitation wavelength 718 nm) during the functionalization process with (a) addition of water (blank sample), and (b) DOC, or (c) Brij35 solutions. The concentration of SWCNTs and PhBr-Dz was the same in all samples. Unmodified (8,6) SWCNTs obtained from HiPco using the described ATPE methodology were used as a reference.

this chirality, as indicated above, without using any additional means of promoting the reaction, prompting us to investigate this case further. This is a multidimensional problem to consider since the extracted SWCNTs we subjected to functionalization came directly from the ATPE process.

Consequently, the sample was not only composed of SWCNTs, surfactant, and water as usual, but also the phase-forming components and partitioning modulators were present. To probe why the studied SWCNTs were relatively reactive, compared to SWCNT mixtures simply suspended with a single surfactant [51], we intentionally added DOC or Brij35 to the reaction mixture and examined the tendency of PhBr-Dz to modify (8,6) SWCNTs. The results showed that the functionalization outcomes were indeed strictly dependent on the sample composition. The addition of DOC blocked functionalization altogether (Fig. 3(b)). Even after 20 h of the process, no sign of E_{11}^* formation could be seen. In contrast, the introduction of Brij35 gave the opposite results, and the functionalization occurred more rapidly in the early stage of the reaction (Fig. 3(c)). Upon the combination of the process mixture with Brij35, a strong E_{11}^* signal was already noted, indicating the implantation of luminescent defects into the structure.

To understand this phenomenon, we need to compare the structures of these surfactants. DOC is more planar and rigid, while Brij35 is linear. The former tends to form dense and tightly packed micelles around SWCNTs [12], which can hamper the functionalization. Moreover, DOC can also create secondary micelles further hindering the approach of PhBr-Dz molecules to the SWCNT surface, preventing the necessary electron transfer to initiate the grafting [52], thus blocking the functionalization. Besides these points, we recently noted that non-ionic surfactants, such as Brij35, show affinity toward larger diameter SWCNTs [12], such as (8,6) SWCNT. As a consequence, it is reasonable to assume that the addition of Brij35 to the mixture replaced DOC on the surface of the (8,6) SWCNTs, decreasing the coverage of the surface, and thereby facilitating functionalization. Brij35 forms more randomly arranged and loosely packed micelles [53], so the SWCNT surface is less tightly protected than it is with DOC, which enables the functionalization to readily occur. After 24 h of the reaction (Fig. S19 in the ESM), the ratio of E_{11}^*/E_{11} was indeed the highest in the case of the Brij35 addition. However, the much higher level of noise suggests that the SWCNTs were probably over-functionalized at this point.

When it became clear that functionalization of larger diameter SWCNTs was possible, our aim was to accelerate this process. The long duration of the reaction makes it more difficult to control and monitor the progress. With this in mind, we decided to use an ultrasonic bath to provide the energy necessary to initiate the reaction. Diazonium salts undergo C–N homolytic bond cleavage in which aryl radicals are formed [54], and these active species react with the SWCNT surface, causing functionalization, so facilitating this process should simplify the covalent modification of SWCNTs. The application of mild sonication allowed us to shorten the process from 2.5 h to just 10 min (Fig. S20(a) in the ESM). The functionalization results were consistent with each other. Interestingly, the DOC shielding effect was so pronounced that even ultrasonic treatment was not able to impair the protective coating around the SWCNTs. As a result, no signs of chemical modification could be seen in this case (Fig. S20(b) in the ESM). On the other hand, the addition of Brij35 reduced the E_{11}^*/E_{11} ratio from 0.8 to 0.6, compared to functionalization without the addition of Brij35 or DOC (Fig. S20(c) in the ESM). Analogously, the E_{11}^*/E_{11} ratio after the 2.5-h long sonication-free treatment was also lower when Brij35 was added (Figs. 3(a) and 3(c)). We attribute this to the fact that the introduction of additional Brij35 into the system caused formation of more densely packed micelles compared with the reference sample, which hindered the access of PhBr-Dz to the surface of the SWCNT. This effect is not observed instantly because the molecules of non-ionic surfactant require a prolonged time to deposit on the SWCNT surface due to their relatively low mobility [12].

To elucidate the influence of surfactants on functionalization, we used a polychiral SWCNT dispersion (HiPco) prepared in an aqueous solution of DOC. This starting material was subjected to PhBr-Dz at various Brij35 concentrations. In the absence of Brij35, this treatment resulted in the quenching of signals from SWCNTs with diameters greater than 0.9 nm (Fig. 4(a) and Fig. S21(a) in the ESM), such as (8,6), (9,4), or (9,5) due to doping of the SWCNTs [55]. It has been reported that redox agents can interact with SWCNTs to either increase or decrease PL intensity [56]. The reason why the SWCNTs above 0.9 nm are susceptible to quenching can be attributed to their smaller band gap [57], which facilitates this effect [58].

Moreover, sonication of the reaction mixture did not alter the PL map, and no clear functionalization signs could be observed (Fig. 4(b)). The still visible (6,5), (7,5), (8,3), and (8,4) SWCNTs had larger band gaps of 2.02, 1.62, 1.08, and 1.13 eV [59], respectively, making them less susceptible to doping. Subsequently, filtration of this material allowed us to wash out the majority of PhBr-Dz present in the solution, and after redispersion of the SWCNTs in the DOC solution, we were able to detect all the chiralities initially present. Nonetheless, the emergence of a small intensity peak at 1134 nm, referred to as E_{11}^* (6,5) SWCNT (Fig. 4(c)), revealed that these SWCNTs were mildly functionalized. We postulate that filtration was not sufficient to remove the diazonium salt molecules adsorbed on the SWCNT surface, which, in turn, decomposed and reacted with (6,5) SWCNTs during redispersion involving sonication. Ultrasonication did not have a noticeable influence on the selectivity of the functionalization.

Next, we analyzed the influence of Brij35 concentration on the course of doping and functionalization. These outcomes were found to be dependent on the concentration of the surfactant. A low dosage (0.037%) caused the disappearance of signals from two chiralities, i.e., (7,5) and (8,4) SWCNTs (diameters of 0.829 and 0.840 nm, respectively), while the larger SWCNTs became slightly more detectable (Fig. 4(d)). Interestingly, when the Brij35 concentration was increased further to 0.074%, and the PhBr-Dz was introduced, the smallest SWCNTs, i.e., (6,5) and (8,3) SWCNTs (diameters of 0.757 and 0.782 nm, respectively) disappeared from the PL map while all other signals remained detectable (Fig. 4(g)). Therefore, we see that the fading of the SWCNTs from the recorded PL excitation–emission maps is Brij35 concentration dependent. The higher the Brij35 concentration, the less apparent the small SWCNTs were. This result was in agreement with our previous findings that Brij35 favors suspension of large-diameter SWCNTs. Therefore, with the increase in Brij35 concentration, larger SWCNTs became more resistant to doping and did not vanish from the PL maps.

Sonication caused the larger SWCNTs to appear in both cases, but at the lower Brij35 concentration (6,5) and (8,3), SWCNTs were detectable, whereas they were quenched with increasing Brij35

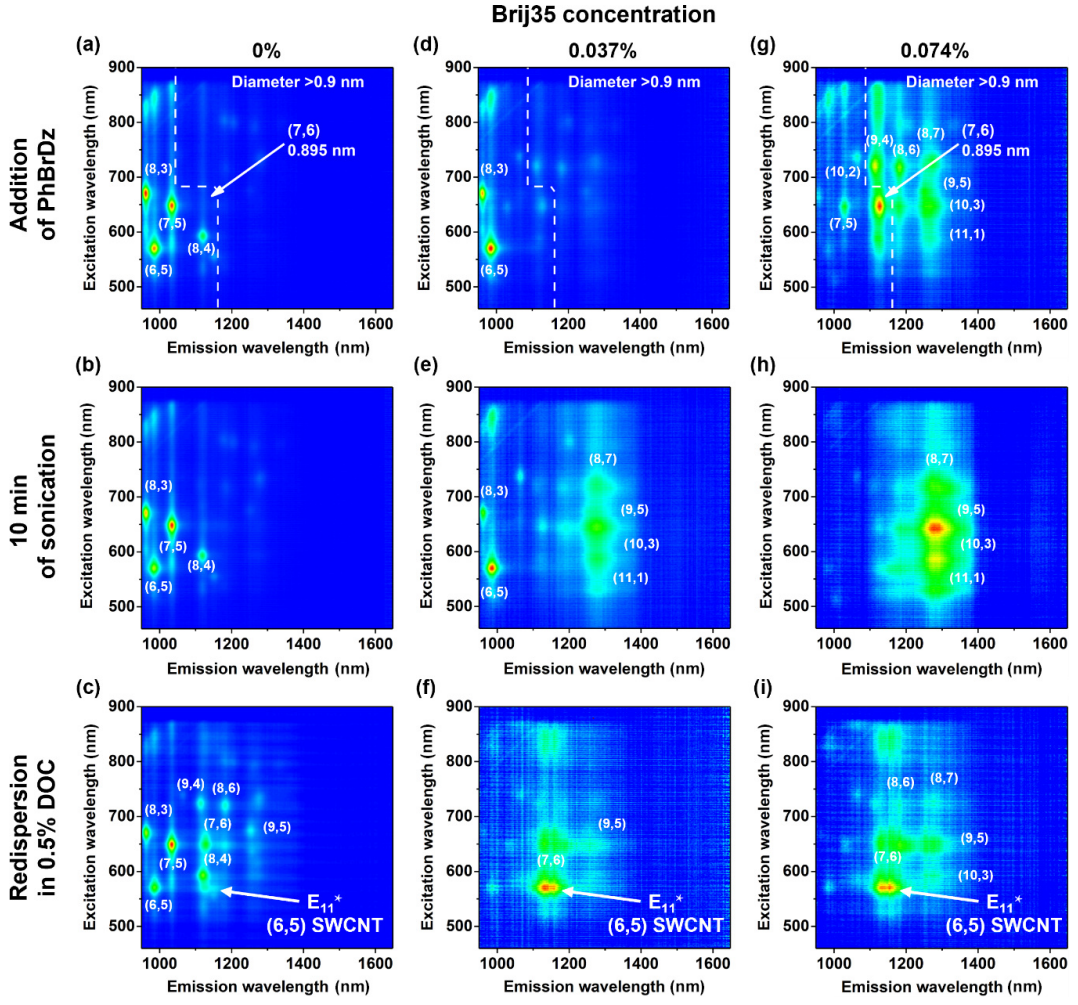

Figure 4 PL excitation–emission maps for a series of experiments using HiPco SWCNTs showing the influence of Brij35 concentration on the course of SWCNT functionalization. (a), (d), and (g) show the PL maps of samples only exposed to PhBr-Dz; (b), (e), and (h) display the effect of chemical modification after 10 min of sonication; and (c), (f), and (i) present PL maps of the second raw samples after removal of the components of chemical modification and redispersion in 0.5% DOC aq. solution.

addition (Figs. 4(e) and 4(h)). Redispersion of the material gave similar results for both concentrations in terms of chemical modification, nearly the same intensity of E_{11}^* (6,5) SWCNT being recorded. The only difference was observed in the intensity values of the other peaks. At the higher concentration of Brij35, larger SWCNTs were more visible once again, confirming the affinity of non-ionic surfactants to large-diameter SWCNTs (Figs. 4(f) and 4(i)).

The results obtained so far confirmed the previously mentioned hypothesis. DOC micelles are tightly packed around smaller SWCNTs, acting as an almost impenetrable barrier for PhBr-Dz. DOC has a lower affinity for larger SWCNTs, so the SWCNTs are only partially covered with it, leaving them vulnerable to PhBr-Dz doping. However, these SWCNTs are less reactive than the small ones, such as (6,5) SWCNTs [47], explaining why they were not functionalized. The addition of Brij35 caused the destabilization of the DOC micelles around smaller SWCNTs. Consequently, the signals of the small-diameter SWCNTs started to quench, whereas those of the larger ones started to appear. One could also consider the existence of mixed micelles of DOC and Brij35, which were reported before [60, 61]. Due to the high curvature of small-diameter SWCNTs, such micelles could allow PhBr-Dz to approach and react with the SWCNT surface. Finally, surfactants with long alkyl chains such as SDS or Brij35, tend to arrange radially around the SWCNT circumference in a loose fashion [12, 62], which should favor SWCNT functionalization (Scheme S2 in the ESM). However, further research is required to describe this phenomenon with certainty.

To make the proposed functionalization technique more controllable, we decided to use (L)-ascorbic acid (VC), which is known for its radical scavenging activity and its ability to react with diazonium salts [63]. The aim was to use it as a functionalization deactivator that would preserve the material from excessive functionalization. The addition of VC to HiPco SWCNTs doped the material, as the PL intensity was reduced by ca. 2.5 times (Figs. S21(a) and 21(b) in the ESM). We noted that mixing of the extracted (8,6) SWCNTs with VC caused a much lower decrease in PL intensity (Figs. S21(c) and S21(d) in the ESM). This is attributed mainly to the decrease in pH, which caused protonation of the carboxylic group of DOC, leading to SWCNT agglomeration and PL intensity reduction (this phenomenon is most evident in Fig. S26 in the ESM, which will be discussed in detail in the ESM). We were, therefore, able to purify the sorted SWCNTs from the post-separation matrix, as described earlier in the text. In contrast, the

isolated (8,6) SWCNTs were primarily covered with Brij35, which is a non-ionic surfactant and thus much more resistant to pH changes. Being less susceptible to protonation, the agglomeration of the SWCNTs was not so severe.

To check the possible interaction of VC with the functionalization mixture, we reproduced the (8,6) SWCNT grafting procedure with both no surfactant and Brij35 addition. In both cases, when VC was present in solution, no sign of reaction was observed in the first 20 h. Surprisingly, after 4 days, a small E_{11}^* signal started to appear, indicating that SWCNT functionalization occurred even in the presence of VC, which was supposed to halt the process (Fig. S22 in the ESM). We hypothesize that diazo-ascorbate ethers can be formed after the addition of VC to diazonium salts at room temperature, which are much more stable in an aqueous environment than diazonium salts [64]. However, this property also makes them less reactive, explaining why it took so much time to implant into the SWCNT side wall to create luminescent sp^3 defects. We were also able to observe the effect of Brij35. The increased concentration of this surfactant resulted in better coverage of the SWCNT surface with its molecules, lowering the ratio of E_{11}^* to E_{11} (from 0.284 to 0.244) by prohibiting access to the SWCNT surface (Fig. S22(b) in the ESM), compared with the sample prepared in the absence of this surfactant (Fig. S22(a) in the ESM). These results were in accordance with earlier findings (Fig. 3). Finally, we examined the effect of VC addition on the optical properties of (8,6) SWCNTs already functionalized with PhBr-Dz. Interestingly, upon VC inclusion, the E_{11}^* peak disappeared, while the intensity of E_{11} doubled (Fig. S23 in the ESM). We are unable to find a satisfactory explanation for this phenomenon at present.

To elucidate this effect, we monitored the reaction progress across a wider timeframe (Fig. 5(a)). After 3 days, we could see that the functionalization progressed, and the E_{11}^* peak gained intensity, reaching the level of the E_{11} peak. We attribute this to a slow decomposition reaction of PhBr-Dz diazoethers formed after the addition of VC to the sample containing PhBr-Dz. The product of this reaction can further react with the SWCNT and introduce sp^3 defects, which causes the E_{11}^* peak to gradually reappear after the initial quenching. Much higher E_{11}^*/E_{11} intensity ratios than in the conventional functionalization routes described above can be attributed to the slow decomposition of the diazoether. Hence, the reaction between the SWCNTs and the generated radicals [63] progresses more steadily, and the termination of the radical process is less likely. Possible homolytic bond cleavage products, which can graft to SWCNTs, are shown in Fig. 5(b). It is also worth noting that the E_{11}^* peak after 14 days shifted from 1304 to around 1320 nm. This suggests that either the sp^3 defect concentration rose significantly or that the structure of the attached groups underwent major changes. However, more research needs to be performed to fully explain this result.

Nonetheless, the (8,6) SWCNT E_{11}^* peak intensity drop after addition of the VC suggests that this material may exhibit sensing properties that can hopefully be utilized for biosensor development. Furthermore, the excitation wavelength (~ 1180 nm), as well as the emission wavelength (~ 1300 nm), fits perfectly in the second

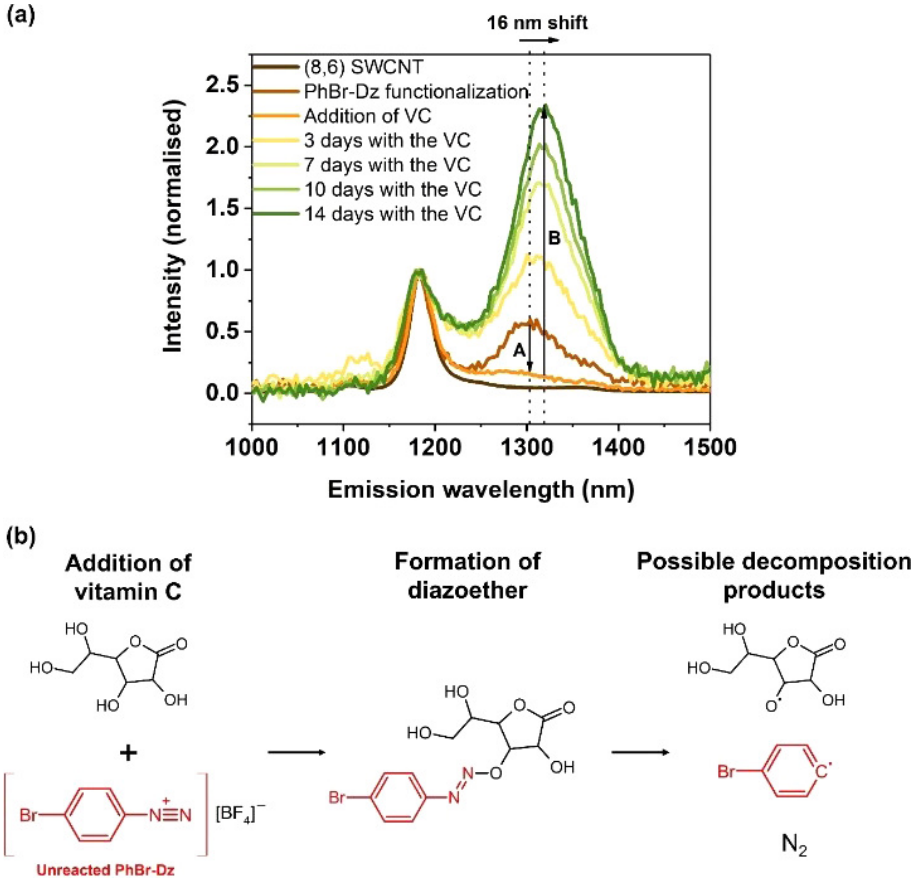

Figure 5 (a) Results of (L)-ascorbic acid addition on optical properties of (8,6) SWCNTs functionalized with PhBr-Dz (excitation wavelength: 718 nm). A–addition of VC, B–14 days of the reaction. (b) Possible route of reaction between the unreacted remaining PhBr-Dz and the added VC. At first, a stable diazoether is formed, which decomposes over time, giving various products, some of which can be added to SWCNTs (some of the possibilities are shown).

biological window. The potential application of SWCNTs as ratiometric sensors has already been examined; however, the most commonly used SWCNT type is (6,5) SWCNT [65, 66]. To the best of our knowledge, the newly developed extraction and functionalization procedure of (8,6) SWCNT allows one of the most redshifted SWCNT to be obtained in good yield for the first time. Further studies are required, because it should be possible to generate the E_{11}^{*-} peak by using more refined grafting agents such as bisdiazonium salts [47].

To interpret the results presented above more thoroughly, we studied the effect of VC addition to HiPco SWCNTs also treated with PhBr-Dz under sonication (Fig. S24(a) in the ESM). After the addition of VC to such SWCNTs, all of the chiralities present in the starting material became detectable (Fig. S24(b) in the ESM). Filtration followed by redispersion in DOC solution further increased the intensities of the peaks from all of the SWCNTs, but also small E_{11}^{*} (6,5) SWCNT signals appeared (Fig. S24(c) in the ESM). This shows that VC is unable to react with all of the PhBr-Dz adsorbed on the surface of the SWCNTs in such a short time, even when the reaction mixture is sonicated. Only the most reactive and smallest nanotubes, the (6,5) SWCNTs, were slightly modified, but this was likely caused by the sonication employed to redisperse the sample after filtration from VC and other components. On the contrary, when Brij35 was added to HiPco SWCNTs, considerable changes to the optical characteristics of the material were registered (Fig. S25 in the ESM). Given the relatively low intensity of the recorded PL peaks, it is clear that the inclusion of Brij35 promoted the grafting of SWCNTs. Consequently, the results indisputably prove that the functionalization's course can be directed by the addition of specific surfactant molecules into the mixture of SWCNTs subjected to chemical modification. Further discussion regarding the interaction of VC with SWCNT is presented in the ESM.

3 Conclusions

ATPE is a very versatile method, which can be tuned by a multitude of interrelated parameters. Consequently, it is possible to adjust the extraction system to harvest desired SWCNT types. The development of simple strategies to isolate specific SWCNTs is important to increase the technological readiness level of this material. However, the composition of the starting raw SWCNT materials often makes such a large impact on the course of the differentiation that the purification strategy must be optimized for each particular case. This hinders progress in the field, especially for researchers whose focus is not centered on studying the nuts and bolts of SWCNT partitioning. In this study, we presented a comprehensive method for processing of SWCNTs, which enabled the enrichment of (8,6) SWCNTs in only three steps from four raw SWCNT materials. The devised strategy is robust and straightforward as it produces (8,6)-enriched SWCNTs from various sources without any changes in the extraction parameters. Interestingly, we found that it is also possible to harvest such species from relatively inexpensive large-diameter SWCNTs, making this approach highly practical. Importantly, the obtained (8,6) SWCNTs have favorable optical properties as their PL emission wavelength is located quite far into the near-infrared range. This can be further enhanced by chemical modification of such SWCNTs, the possibility of which has been examined in detail herein. The fact that the emission from these SWCNTs coincides with the optical window of tissue transparency means that these SWCNTs are highly valuable assets for application in nanomedicine. In particular, the observed interaction between functionalized (8,6) SWCNT and VC gives hope to the possibility of using this material in ratiometric sensing of other analytes.

Finally, we also showed the opportunities for precise isolation of specific SWCNTs from large-diameter SWCNT raw material containing numerous SWCNT species. We also presented how such materials can be purified from the post-separation matrix. The designed purification method was effective as it enabled suspension of the isolated material in an organic solvent using a conjugated polymer without any issues. Consequently, this technique may facilitate the utilization of SWCNTs sorted in aqueous media in the production of SWCNT-based devices commonly made using organic solvents, which cannot be used in the ATPE process.

4 Experimental

All the information about the materials and methods was provided in the ESM.

Electronic Supplementary Material: Supplementary material (description of materials/methods and results of SWCNT chracterization) is available in the online version of this article at https://doi.org/10.26599/NR.2025.94907112.

Data availability

All data needed to support the conclusions in the paper are presented in the manuscript and the Electronic Supplementary Material. Additional data related to this paper may be requested from the corresponding author upon request.

Acknowledgements

The authors would like to thank the National Science Centre, Poland (under the OPUS program, Grant agreement 2019/33/B/ST5/00631), for financial support of the research. The contribution of Mr. Dominik Just is appreciated.

Declaration of competing interest

All the contributing authors report no conflict of interests in this work.

Author contribution statement

B. P.: Conceptualization, methodology, investigation, visualization, formal analysis, writing – original draft. Ł. C.: Conceptualization, methodology, investigation, visualization, formal analysis, writing – original draft. P. T.: Investigation, formal analysis. L. Y. Z.: Methodology, investigation, visualization. F. Y.: Methodology, resources, writing – review & editing. D. J.: Conceptualization, methodology, validation, formal analysis, resources, supervision, writing-review and editing.

Use of AI statement

AI was not used for the preparation of this work.

References

[1] Iijima, S. Helical microtubules of graphitic carbon. *Nature* **1991**, *354*, 56–58.

[2] Janas, D. Towards monochiral carbon nanotubes: A review of

progress in the sorting of single-walled carbon nanotubes. *Mater. Chem. Front.* **2018**, *2*, 36–63.
[3] Qiu, L.; Ding, F. Understanding single-walled carbon nanotube growth for chirality controllable synthesis. *Acc. Mater. Res.* **2021**, *2*, 828–841.
[4] Tanaka, T.; Jin, H. H.; Miyata, Y.; Kataura, H. High-yield separation of metallic and semiconducting single-wall carbon nanotubes by agarose gel electrophoresis. *Appl. Phys. Express* **2008**, *1*, 114001.
[5] Arnold, M. S.; Green, A. A.; Hulvat, J. F.; Stupp, S. I.; Hersam, M. C. Sorting carbon nanotubes by electronic structure using density differentiation. *Nat. Nanotechnol.* **2006**, *1*, 60–65.
[6] Dzienia, A.; Just, D.; Taborowska, P.; Mielanczyk, A.; Milowska, K. Z.; Yorozuya, S.; Naka, S.; Shiraki, T.; Janas, D. Mixed-solvent engineering as a way around the trade-off between yield and purity of (7,3) single-walled carbon nanotubes obtained using conjugated polymer extraction. *Small* **2023**, *19*, 2304211.
[7] Flavel, B. S.; Moore, K. E.; Pfohl, M.; Kappes, M. M.; Hennrich, F. Separation of single-walled carbon nanotubes with a gel permeation chromatography system. *ACS Nano* **2014**, *8*, 1817–1826.
[8] Fagan, J. A. Aqueous two-polymer phase extraction of single-wall carbon nanotubes using surfactants. *Nanoscale Adv.* **2019**, *1*, 3307–3324.
[9] Pereira, J. F. B.; Coutinho, J. A. P. Aqueous two-phase systems. In *Liquid-Phase Extraction*. Poole, C. F.; Elsevier: Amsterdam, 2020; pp. 157–182.
[10] Iqbal, M.; Tao, Y. F.; Xie, S. Y.; Zhu, Y. F.; Chen, D. M.; Wang, X.; Huang, L. L.; Peng, D. P.; Sattar, A.; Shabbir, M. A. B. et al. Aqueous Two-Phase System (ATPS): An overview and advances in its applications. *Biol. Proced. Online* **2016**, *18*, 18.
[11] Podlesny, B.; Gaida, B.; Brzeczek-Szafran, A.; Chrobok, A.; Janas, D. Partitioning of SWCNT mixtures using amphiphilic carbohydrate-based surfactants. *Sep. Purif. Technol.* **2024**, *343*, 127120.
[12] Podlesny, B.; Hinkle, K. R.; Hayashi, K.; Niidome, Y.; Shiraki, T.; Janas, D. Highly-selective harvesting of (6,4) SWCNTs using the aqueous two-phase extraction method and nonionic surfactants. *Adv. Sci.* **2023**, *10*, 2207218.
[13] Podlesny, B.; Olszewska, B.; Yaari, Z.; Jena, P. V.; Ghahramani, G.; Feiner, R.; Heller, D. A.; Janas, D. En route to single-step, two-phase purification of carbon nanotubes facilitated by high-throughput spectroscopy. *Sci. Rep.* **2021**, *11*, 10618.
[14] Fagan, J. A.; Hároz, E. H.; Ihly, R.; Gui, H.; Blackburn, J. L.; Simpson, J. R.; Lam, S.; Hight Walker, A. R.; Doorn, S. K.; Zheng, M. Isolation of > 1 nm diameter single-wall carbon nanotube species using aqueous two-phase extraction. *ACS Nano* **2015**, *9*, 5377–5390.
[15] Podlesny, B.; Shiraki, T.; Janas, D. One-step sorting of single-walled carbon nanotubes using aqueous two-phase extraction in the presence of basic salts. *Sci. Rep.* **2020**, *10*, 9250.
[16] Wei, L.; Liu, B. L.; Wang, X. T.; Gui, H.; Yuan, Y.; Zhai, S. L.; Ng, A. K.; Zhou, C. W.; Chen, Y. (9,8) Single-walled carbon nanotube enrichment via aqueous two-phase separation and their thin-film transistor applications. *Adv. Electron. Mater.* **2015**, *1*, 1500151.
[17] Turek, E.; Shiraki, T.; Shiraishi, T.; Shiga, T.; Fujigaya, T.; Janas, D. Single-step isolation of carbon nanotubes with narrow-band light emission characteristics. *Sci. Rep.* **2019**, *9*, 535.
[18] Li, H.; Gordeev, G.; Garrity, O.; Peyyety, N. A.; Selvasundaram, P. B.; Dehm, S.; Krupke, R.; Cambré, S.; Wenseleers, W.; Reich, S. et al. Separation of specific single-enantiomer single-wall carbon nanotubes in the large-diameter regime. *ACS Nano* **2020**, *14*, 948–963.
[19] Podlesny, B.; Kumanek, B.; Borah, A.; Yamaguchi, R.; Shiraki, T.; Fujigaya, T.; Janas, D. Thermoelectric properties of thin films from sorted single-walled carbon nanotubes. *Materials* **2020**, *13*, 3808.
[20] Tambasov, I. A.; Voronin, A. S.; Evsevskaya, N. P.; Volochaev, M. N.; Fadeev, Y. V.; Simunin, M. M.; Aleksandrovsky, A. S.; Smolyarova, T. E.; Abelian, S. R.; Tambasova, E. V. et al. Thermoelectric properties of low-cost transparent single wall carbon nanotube thin films obtained by vacuum filtration. *Phys. E: Low-Dimens. Syst. Nanostructures* **2019**, *114*, 113619.
[21] Li, H.; Gordeev, G.; Garrity, O.; Reich, S.; Flavel, B. S. Separation of small-diameter single-walled carbon nanotubes in one to three steps with aqueous two-phase extraction. *ACS Nano* **2019**, *13*, 2567.
[22] Tu, X. M.; Manohar, S.; Jagota, A.; Zheng, M. DNA sequence motifs for structure-specific recognition and separation of carbon nanotubes. *Nature* **2009**, *460*, 250–253.
[23] Fagan, J. A.; Khripin, C. Y.; Silvera Batista, C. A.; Simpson, J. R.; Hároz, E. H.; Hight Walker, A. R.; Zheng, M. Isolation of specific small-diameter single-wall carbon nanotube species via aqueous two-phase extraction. *Adv. Mater.* **2014**, *26*, 2800–2804.
[24] Ao, G. Y.; Streit, J. K.; Fagan, J. A.; Zheng, M. Differentiating left- and right-handed carbon nanotubes by DNA. *J. Am. Chem. Soc.* **2016**, *138*, 16677–16685.
[25] Sims, C. M.; Fagan, J. A. Surfactant chemistry and polymer choice affect single-wall carbon nanotube extraction conditions in aqueous two-polymer phase extraction. *Carbon* **2022**, *191*, 215–226.
[26] Turek, E.; Kumanek, B.; Boncel, S.; Janas, D. Manufacture of networks from large diameter single-walled carbon nanotubes of particular electrical character. *Nanomaterials* **2019**, *9*, 614.
[27] Omachi, H.; Komuro, T.; Matsumoto, K.; Nakajima, M.; Watanabe, H.; Hirotani, J.; Ohno, Y.; Shinohara, H. Aqueous two-phase extraction of semiconducting single-wall carbon nanotubes with isomaltodextrin and thin-film transistor applications. *Appl. Phys. Express* **2019**, *12*, 097003.
[28] Cao, L. T.; Li, Y. H.; Liu, Y.; Zhao, J. T.; Nan, Z. Y.; Xiao, W. X.; Qiu, S.; Kang, L. X.; Jin, H. H.; Li, Q. W. Iterative strategy for sorting single-chirality single-walled carbon nanotubes from aqueous to organic systems. *ACS Nano* **2024**, *18*, 3783–3790.
[29] Luo, X.; Wei, X. J.; Liu, L.; Yao, Z. H.; Xiong, F. B.; Zhou, W. Y.; Xie, S. S.; Liu, H. P. One-step separation of high-purity single-chirality single-wall carbon nanotubes using sodium hyodeoxycholate. *Carbon* **2023**, *207*, 129–135.
[30] Just, D.; Dzienia, A.; Milowska, K. Z.; Mielańczyk, A.; Janas, D. High-yield and chirality-selective isolation of single-walled carbon nanotubes using conjugated polymers and small molecular chaperones. *Mater. Horiz.* **2024**, *11*, 758–767.
[31] Dzienia, A.; Just, D.; Wasiak, T.; Milowska, K. Z.; Mielańczyk, A.; Labedzki, N.; Kruss, S.; Janas, D. Size matters in conjugated polymer chirality-selective SWCNT extraction. *Adv. Sci.* **2024**, 202402176.
[32] Li, Y. H.; Zheng, M. M.; Yao, J.; Gong, W. B.; Li, Y. J.; Tang, J. S.; Feng, S.; Han, R. Y.; Sui, Q.; Qiu, S. et al. High-purity monochiral carbon nanotubes with a 1.2 nm diameter for high-performance field-effect transistors. *Adv. Funct. Mater.* **2022**, *32*, 2107119.
[33] Berton, N.; Lemasson, F.; Poschlad, A.; Meded, V.; Tristram, F.; Wenzel, W.; Hennrich, F.; Kappes, M. M.; Mayor, M. Selective dispersion of large-diameter semiconducting single-walled carbon nanotubes with pyridine-containing copolymers. *Small* **2014**, *10*, 360–367.
[34] Lei, T.; Lai, Y. C.; Hong, G. S.; Wang, H. L.; Hayoz, P.; Weitz, R. T.; Chen, C. X.; Dai, H. J.; Bao, Z. N. Diketopyrrolopyrrole (DPP)-based donor-acceptor polymers for selective dispersion of large-diameter semiconducting carbon nanotubes. *Small* **2015**, *11*, 2946–2954.
[35] Tange, M.; Okazaki, T.; Iijima, S. Selective extraction of large-diameter single-wall carbon nanotubes with specific chiral indices by poly(9,9-dioctylfluorene-alt-benzothiadiazole). *J. Am. Chem. Soc.* **2011**, *133*, 11908–11911.
[36] Zhang, P.; Yi, W. H.; Bai, L.; Tian, Y. L.; Hou, J.; Jin, W. Q.; Si, J. H.; Hou, X. Enrichment of large-diameter semiconducting single-walled carbon nanotubes by a mixed-extractor strategy. *Chem. - Asian J.* **2019**, *14*, 3855–3862.
[37] Li, Y. H.; Liu, Y.; Jin, F.; Cao, L. T.; Jin, H. H.; Qiu, S.; Li, Q. W. Polymer removal and dispersion exchange of (10,5) chiral carbon nanotubes with enhanced 1.5 μm photoluminescence. *Nanoscale Adv.* **2024**, *6*, 792–797.
[38] Diao, S.; Hong, G. S.; Robinson, J. T.; Jiao, L. Y.; Antaris, A. L.; Wu,

J. Z.; Choi, C. L.; Dai, H. J. Chirality enriched (12,1) and (11,3) single-walled carbon nanotubes for biological imaging. *J. Am. Chem. Soc.* **2012**, *134*, 16971–16974.

[39] Welsher, K.; Liu, Z.; Sherlock, S. P.; Robinson, J. T.; Chen, Z.; Daranciang, D.; Dai, H. J. A route to brightly fluorescent carbon nanotubes for near-infrared imaging in mice. *Nat. Nanotechnol.* **2009**, *4*, 773–780.

[40] TUBALL™ graphene nanotubes[Online]. https://tuball.com/about-tuball (accessed Jul 27, 2024).

[41] Tsyboulski, D. A.; Rocha, J. D. R.; Bachilo, S. M.; Cognet, L.; Weisman, R. B. Structure-dependent fluorescence efficiencies of individual single-walled carbon nanotubes. *Nano Lett.* **2007**, *7*, 3080–3085.

[42] Jorio, A.; Saito, R. Raman spectroscopy for carbon nanotube applications. *J. Appl. Phys.* **2021**, *129*, 021102.

[43] Yang, F.; Wang, M.; Zhang, D. Q.; Yang, J.; Zheng, M.; Li, Y. Chirality pure carbon nanotubes: Growth, sorting, and characterization. *Chem. Rev.* **2020**, *120*, 2693–2758.

[44] Smith, A. M.; Mancini, M. C.; Nie, S. M. Second window for *in vivo* imaging. *Nat. Nanotechnol.* **2009**, *4*, 710–711.

[45] Pekker, Á.; Kamarás, K. Wide-range optical studies on various single-walled carbon nanotubes: Origin of the low-energy gap. *Phys. Rev. B* **2011**, *84*, 075475.

[46] Li, Y. D.; Rahman, A. F. M. M.; Liu, G.; Xiong, Z. C.; Koezuka, K.; Xu, Z. G.; Komatsu, N.; Wang, F. Enrichment of large-diameter single-walled carbon nanotubes (SWNTs) with metallo-octaethylporphyrins. *Materials* **2013**, *6*, 3064–3078.

[47] Janas, D. Perfectly imperfect: A review of chemical tools for exciton engineering in single-walled carbon nanotubes. *Mater. Horiz.* **2020**, *7*, 2860–2881.

[48] Yu, B. D.; Naka, S.; Aoki, H.; Kato, K.; Yamashita, D.; Fujii, S.; Kato, Y. K.; Fujigaya, T.; Shiraki, T. Ortho-substituted aryldiazonium design for the defect configuration-controlled photoluminescent functionalization of chiral single-walled carbon nanotubes. *ACS Nano* **2022**, *16*, 21452–21461.

[49] Paschotta, R. Optical fiber communications. In *RP Photonics Encyclopedia*. RP Photonics AG, 2005. https://www.rp-photonics.com/optical_fiber_communications.html (accessed July 27, 2024).

[50] Berger, F. J.; Lüttgens, J.; Nowack, T.; Kutsch, T.; Lindenthal, S.; Kistner, L.; Müller, C. C.; Bongartz, L. M.; Lumsargis, V. A.; Zakharko, Y. et al. Brightening of long, polymer-wrapped carbon nanotubes by sp^3 functionalization in organic solvents. *ACS Nano* **2019**, *13*, 9259–9269.

[51] He, X. W.; Hartmann, N. F.; Ma, X. D.; Kim, Y.; Ihly, R.; Blackburn, J. L.; Gao, W. L.; Kono, J.; Yomogida, Y.; Hirano, A. et al. Tunable room-temperature single-photon emission at telecom wavelengths from sp^3 defects in carbon nanotubes. *Nat. Photonics* **2017**, *11*, 577–582.

[52] Hilmer, A. J.; McNicholas, T. P.; Lin, S. C.; Zhang, J. Q.; Wang, Q. H.; Mendenhall, J. D.; Song, C.; Heller, D. A.; Barone, P. W.; Blankschtein, D. et al. Role of adsorbed surfactant in the reaction of aryl diazonium salts with single-walled carbon nanotubes. *Langmuir* **2012**, *28*, 1309–1321.

[53] Blanch, A. J.; Lenehan, C. E.; Quinton, J. S. Dispersant effects in the selective reaction of aryl diazonium salts with single-walled carbon nanotubes in aqueous solution. *J. Phys. Chem. C* **2012**, *116*, 1709–1723.

[54] Rehorek, D.; Janzen, E. G. Spin-trapping von radikalen bei der zersetzung aromatischer diazoniumsalze mittels ultraschall. *J. für Prakt. Chem.* **1984**, *326*, 935–940.

[55] O'Connell, M. J.; Eibergen, E. E.; Doorn, S. K. Chiral selectivity in the charge-transfer bleaching of single-walled carbon-nanotube spectra. *Nat. Mater.* **2005**, *4*, 412–418.

[56] Hou, Z. T.; Krauss, T. D. Photoluminescence brightening of isolated single-walled carbon nanotubes. *J. Phys. Chem. Lett.* **2017**, *8*, 4954–4959.

[57] Kataura, H.; Kumazawa, Y.; Maniwa, Y.; Umezu, I.; Suzuki, S.; Ohtsuka, Y.; Achiba, Y. Optical properties of single-wall carbon nanotubes. *Synth. Met.* **1999**, *103*, 2555–2558.

[58] Kumanek, B.; Milowska, K. Z.; Przypis, Ł.; Stando, G.; Matuszek, K.; MacFarlane, D.; Payne, M. C.; Janas, D. Doping Engineering of single-walled carbon nanotubes by nitrogen compounds using basicity and alignment. *ACS Appl. Mater. Interfaces* **2022**, *14*, 25861–25877.

[59] Liu, K. H.; Deslippe, J.; Xiao, F. J.; Capaz, R. B.; Hong, X. P.; Aloni, S.; Zettl, A.; Wang, W. L.; Bai, X. D.; Louie, S. G. et al. An atlas of carbon nanotube optical transitions. *Nat. Nanotechnol.* **2012**, *7*, 325–329.

[60] Haque, M. E.; Das, A. R.; Moulik, S. P. Mixed micelles of sodium deoxycholate and polyoxyethylene sorbitan monooleate (Tween 80). *J. Colloid Interface Sci.* **1999**, *217*, 1–7.

[61] Hsieh, Y. Z.; Kuo, K. L. Separation of retinoids by micellar electrokinetic capillary chromatography. *J. Chromatogr. A* **1997**, *761*, 307–313.

[62] Tiwari, P.; Podleśny, B.; Krzywiecki, M.; Milowska, K. Z.; Janas, D. Understanding the partitioning behavior of single-walled carbon nanotubes using an aqueous two-phase extraction system composed of non-ionic surfactants and polymers. *Nanoscale Horiz.* **2023**, *8*, 685–694.

[63] Costas-Costas, U.; Gonzalez-Romero, E.; Bravo-Diaz, C. Effects of ascorbic acid on arenediazonium salts reactivity: Kinetics and mechanism of the reaction. *Helv. Chim. Acta* **2001**, *84*, 632–648.

[64] Doyle, M. P.; Nesloney, C. L.; Shanklin, M. S.; Marsh, C. A.; Brown, K. C. Formation and characterization of 3-O-arenediazoascorbic acids. New stable diazo ethers. *J. Org. Chem.* **1989**, *54*, 3785–3789.

[65] Settele, S.; Schrage, C. A.; Jung, S.; Michel, E.; Li, H.; Flavel, B. S.; Hashmi, A. S. K.; Kruss, S.; Zaumseil, J. Ratiometric Fluorescent sensing of pyrophosphate with sp^3-functionalized single-walled carbon nanotubes. *Nat. Commun.* **2024**, *15*, 706.

[66] Ma, C.; Mohr, J. M.; Lauer, G.; Metternich, J. T.; Neutsch, K.; Ziebarth, T.; Reiner, A.; Kruss, S. Ratiometric imaging of catecholamine neurotransmitters with nanosensors. *Nano Lett.* **2024**, *24*, 2400–2407.